Cell Biology International ISSN 1065-6995
doi: 10.1002/cbin.11219

RESEARCH ARTICLE

Single amino acid mutations in the *Saccharomyces cerevisiae* rhomboid peptidase, Pcp1p, alter mitochondrial morphology

Mary Elizabeth Huddleston, Ningyu Xiao, Andries Pieter Both and Donna M. Gordon*

Department of Biological Sciences, Mississippi State University, Mississippi State, Mississippi, 39762, USA

Abstract

Key to mitochondrial activities is the maintenance of mitochondrial morphology, specifically cristae structures formed by the invagination of the inner membrane that are enriched in proteins of the electron transport chain. In *Saccharomyces cerevisiae* , these cristae folds are a result of the membrane fusion activities of Mgm1p and the membrane-bending properties of adenosine triphosphate (ATP) synthase oligomerization. An additional protein linked to mitochondrial morphology is Pcp1p, a serine protease responsible for the proteolytic processing of Mgm1p. Here, we have used hydroxylamine-based random mutagenesis to identify amino acids important for Pcp1p peptidase activity. Using this approach we have isolated five single amino acid mutants that exhibit respiratory growth defects that correlate with loss of mitochondrial genome stability. Reduced Pcp1p protease activity was confirmed by immunoblotting with the accumulation of improperly processed Mgm1p. Ultra-structural analysis of mitochondrial morphology in these mutants found a varying degree of defects in cristae organization. However, not all of the mutants presented with decreased ATP synthase complex assembly as determined by blue native polyacrylamide gel electrophoresis. Together, these data suggest that there is a threshold level of processed Mgm1p required to maintain ATP synthase super-complex assembly and mitochondrial cristae organization.

Keywords: ATP synthase; blue native-PAGE; cristae structure; mitochondrial morphology; Pcp1p; peptidase activity

Introduction

In eukaryotic cells, mitochondria are important organelles involved in the production of energy in the form of adenosine triphosphate (ATP), apoptosis, and calcium regulation (Chandel, 2014). The maintenance of mitochondria morphology is integral to these functions (Sun et al., 2007; Cogliati et al., 2013). The structure of mitochondria in wild-type *Saccharomyces cerevisiae* cells is that of a tubular network that extends around the cell periphery (Nunnari et al., 1997; Rafelski et al., 2012). The ultra-structure of mitochondria generally consists of an outer membrane, an inner membrane that folds to form cristae, an intermembrane space, and the matrix. The inner membrane comes in close contact with the outer membrane before folding into cristae, with the area at the base of the cristae fold known as a cristae junction (Mannella et al., 2008; Zick et al., 2009b). A number of proteins embedded in the inner membrane are key to maintaining mitochondrial morphology via regulated fusion and fission-based events. Fusion of the outer and inner membranes with neighboring mitochondria forms the reticular network found in normal yeast cells and fission allows for the partitioning of mitochondria into daughter cells during cellular division (Nunnari et al., 1997). A balance between fusion and fission events is required for the maintenance of mitochondrial structure. For example, cells lacking expression of Dnm1p, a protein responsible for fission of the outer membrane, results in a large, branched mitochondrial network. In contrast, deletion of a protein involved in outer membrane fusion, Fzo1, results in fragmented mitochondria (Sesaki and Jensen, 1999). However, these defects in morphology can be overcome if the opposing activity is removed, as evidenced by the double Δ*fzo1* Δ*dnm1* cells containing normal mitochondria (Sesaki and Jensen, 1999). Fusion

*Corresponding author: e-mail: gordon@biology.msstate.edu
Present address: Human Performance Wing Molecular Mechanisms Branch, Air Force Research Laboratory, Wright Patterson AFB, OH 45433, USA.
Present address: Institute for Stem Cell Biology and Regenerative Medicine, Stanford University School of Medicine, Stanford, CA 94305, USA.
Abbreviations: BN-PAGE, blue native polyacrylamide gel electrophoresis; mtDNA, mitochondrial DNA; TEM, transmission electron microscopy

Cell Biol Int **44** (2020) 200–215 © 2019 The Authors. *Cell Biology International* published by John Wiley & Sons Ltd on behalf of International Federation of Cell Biology

and fission of the inner membrane can also direct cristae formation. Under the stress of induced matrix swelling, fusion of the inner membrane results in very few cristae junctions and large intra-cristae spaces. Upon retraction, most cristae returned to their normal state while some mitochondria contained inner membrane vesicles that are hypothesized to result from fission of those large cristae structures observed during swelling (Mannella et al., 2008). Cristae structures have also been shown to be lost during the progression of apoptosis (Sun et al., 2007).

In *S. cerevisiae*, Pcp1p is a multispanning transmembrane protein of the mitochondrial inner membrane. As a serine protease, Pcp1p cleaves substrate proteins within the membrane environment, an activity linked to regulating mitochondrial structure (Herlan et al., 2003; McQuibban et al., 2003; Sesaki et al., 2003a). Pcp1p has two known substrates: cytochrome *c* peroxidase, or Ccp1p (Esser et al., 2002; Michaelis et al., 2005), and the dynamin-like GTPase, Mgm1p (Wong et al., 2000; Herlan et al., 2003; McQuibban et al., 2003; Wong et al., 2003; Sesaki et al., 2003a). Ccp1p, functions in the reduction of cytochrome *c* to oxidize H_2O_2 (Yonetani and Ohnishi, 1966) which is toxic to cells and can build up as a by-product of oxidative phosphorylation. The second substrate, Mgm1p, has been shown to be required for mitochondrial fusion (Wong et al., 2000, 2003) as cells deleted for *MGM1* give rise to fragmented mitochondria, lose mitochondrial DNA (mtDNA) (Guan et al., 1993; Herlan et al., 2004), and lack cristae ultrastructure (Sesaki et al., 2003b; Amutha et al., 2004). Deletion of *PCP1* also leads to fragmented mitochondria, mitochondria absent of cristae, loss of mtDNA, as well as the inability to grow on nonfermentable carbon sources (McQuibban et al., 2003; Sesaki et al., 2003a) all of which is a result of the inability of these cells to process Mgm1p.

ATP synthase is another protein located within the mitochondria inner membrane with a role in mitochondrial cristae maintenance. This protein complex uses the proton gradient generated by electron transport chain activity for ATP generation. It is composed of a catalytic F_1 "head" found on the matrix side of the inner membrane and a F_0 stalk that is embedded in the inner membrane. The majority of the ATP synthase subunits are encoded by nuclear DNA with the exception of three F_0 subunits (ATP6, ATP8, and ATP9), which are encoded on the mitochondrial genome (Ackerman and Tzagoloff, 2005). The ATP synthase complex contains several proteins that aid in the association between the F_0 and F_1 complexes as well as those that promote the formation of ATP synthase dimers and higher-order oligomers (Arnold et al., 1998; Arselin et al., 2003; Amutha et al., 2004; Wagner et al., 2010). Recent work has shown that the formation of the ATP synthase super-complex is crucial to cristae structure (Arselin et al., 2003; Thomas et al., 2008; Davies et al., 2012). Tim11p, or subunit *e* of ATP synthase, has been shown to be one of the components required for ATP synthase dimerization (Arnold et al., 1997; Arselin et al., 2003; Everard-Gigot et al., 2005). Deletion of *TIM11* leads to fragmented mitochondria that display "onion-like" cristae and an increased tendency to lose mtDNA (Giraud et al., 2002; Paumard et al., 2002; Arselin et al., 2003). F_1F_0 ATP synthase monomers are linked together through Tim11p at the base of the stalk. These dimers then assemble to form higher-order oligomers, which promote inner membrane bending to form the rim of the cristae (Arselin et al., 2003; Thomas et al., 2008; Davies et al., 2012). The observation that Tim11p is not detectable in *mgm1* or *pcp1* deletion mutants (Amutha et al., 2004) suggests a possible connection between mitochondria structure and function influenced directly or indirectly by Pcp1p activity.

In this study, we have generated *pcp1* mutants that contain single amino acid changes that result in a range of catalytic activities in vivo. It was determined by transmission electron microscopy (TEM) and blue native polyacrylamide gel electrophoresis (BN-PAGE) that the ability of each mutant to process Mgm1p correlates with mitochondrial architecture but not necessarily ATP synthase oligomerization. Given the established link between ATP synthase complex assembly and mitochondrial cristae formation, these mutants can be used to dissect the relationship among Pcp1p peptidase activity, Mgm1p-mediated inner membrane fusion, and mitochondrial architecture independent of ATP synthase.

Materials and methods

Strains, media, and reagents

All yeast strains used in this study were derived from BY4741 (*Mata his3Δ1 leu2Δ0 met15Δ0 ura3Δ0*) (Thermo Fisher Scientific). A *pcp1* shuffle strain was constructed by targeted integration, in which the *PCP1* open-reading frame was disrupted with the introduction of *LEU2* (pRS405) as described (Rothstein, 1991). Correct integration was confirmed by genomic polymerase chain reaction (PCR) and the resulting diploid transformed with a *URA3*-marked *PCP1* plasmid, sporulated, and micro-dissected. Covered γ*pcp1*::*LEU2* haploid mutants were identified by growth on uracil and leucine-deficient selective plates.

An epitope-tagged versions of *MGM1* were generated by homologous recombination using a PCR-based approach as described (Longtine et al., 1998). Transformants capable of growth on 0.2 g/L G418 YPD plates were confirmed by genomic PCR analysis.

Yeast media was prepared according to the methods previously described (Sherman, 1991). To ensure retention

of a *HIS3*-marked plasmid, strains were grown in supplemented 0.67% yeast nitrogen base lacking histidine (-His) and containing 2% glucose, 2% raffinose, or 2% ethanol and 3% glycerol as a carbon source. The Δ*tim11* strain was grown in YP media (2% peptone, 1% yeast extract, 2% carbon source). Strains for TEM analysis were grown in histidine-selective media containing 2% raffinose.

pcp1 mutant generation

The *pcp1* mutants were generated by random mutagenesis of a plasmid-based copy of the *PCP1* open-reading frame under the endogenous *PCP1* promoter in the *HIS3*-marked pRS413 vector. Nearly, 500 ng of purified plasmid (DG295) was treated with 1 M hydroxylamine hydrochloride in 0.45 M sodium hydroxide for 20 and 25 h at 37°C (Rose and Fink, 1987). The reaction was stopped with the purification of the plasmid using the Qiagen miniprep kit according to the manufacturer's instructions. The resulting pool of mutagenized plasmid was transformed into the *PCP1* shuffle strain (DGY43) (Schiestl and Gietz, 1989). For identification of mutants, the covering wild-type *PCP1* plasmid was removed by 3 days of growth on 5-fluoroorotic acid (5-FOA)-containing plates (Sherman, 1991). Loss of the *PCP1* URA3-marked plasmid was confirmed as no growth on Uracil plates. Defects in Pcp1p activity were selected as poor growth after replica printing to ethanol/glycerol-based plates.

Plasmids were isolated from the cultures grown overnight at 30°C in 5 mL of selective media as follows. Cells isolated by centrifugation were pretreated in 100 mM Tris pH 9.0 for 10 min at 30°C prior to spheroplast formation in spheroplast buffer (1 M sorbitol, 20 mM Tris pH 7.5, 10 mM ethylenediaminetetraacetic acid (EDTA) pH 8.0; 0.15 μg/μL 100 T zymolyase, and 0.2% β mercapto-ethanol) for 1 h at 30°C. Spheroplasts were isolated by centrifugation at 2,000*g* for 10 min, resuspended Qiagen P1 buffer, and subjected to two freeze-thaw cycles. Spheroplasts were mechanically lysed by vortexing with glass bead. Qiagen P2 buffer was added and incubated at room temperature for 5 min. Qiagen N3 buffer was added and the lysate clarified by centrifugation at 21,130*g* for 10 min. Plasmid DNA was isolated by isopropanol precipitation and used to transform NEB Turbo competent *Escherichia coli* (New England Biolabs). Nucleotide mutations were identified by Sanger sequencing using four primer pair sets that covered the *PCP1* promoter and open-reading frame (Arizona State University, CLAS DNA Laboratory). Following sequencing, all mutants were found to contain a common T962C nucleotide change that resulted in a Valine to Alanine mutation at amino acid position 321. This mutation was also found in the original plasmid and was determined to have no impact on Pcp1p activities (data not shown). When possible, a site-directed mutagenesis approach was used to correct this nucleotide mutation (QuikChange II; Agilent).

Serial dilution spotting assay

Nearly 10^7 cells from exponentially growing cultures were isolated by centrifugation and the resulting cell pellet was resuspended at 10^5 cell/μL in sterile water. Cells were placed in the first column of a 96-well microtiter plate and serially diluted 10-fold by transferring 20 μl cells to 180 μl media. Three microliters from each well were spotted onto selective plates and growth recorded after 3 days at 30°C.

Petite frequency determination

For each strain, a volume of overnight culture equivalent to 10^7 cells was brought up to 1 mL in selective glucose media and serially diluted to achieve 1,000 cells/mL. Multiple 100 μL aliquots were plated onto -His glucose plates. After 3 days at 30°C, the numbers of colonies on each plate were counted and the colonies replica printed onto -His ethanol/glycerol plates. Colonies that grew on -His ethanol/glycerol plates were counted after an additional 3 days of growth at 30°C. This process was independently repeated five times for each strain. The petite frequency was calculated using the following equation: (colony number on glucose−the colony number on ethanol/glycerol)/colony number on glucose × 100.

mtDNA detection by 4′,6-diamidino-2-pheynlindole (DAPI) staining

The cultures were grown overnight in a selective media at 30°C and fixed in 3.7% formaldehyde for 2 h at room temperature. The cells were isolated by centrifugation, washed with sterile distilled water, and resuspended in 50 mM phosphate-buffered saline (PBS) pH 7.4. Permeabilization was carried out in 70% ethanol on ice for 30 min, cells isolated by centrifugation, and the cell pellet resuspended in PBS. DAPI was added at 50 μg/mL for 5 min on ice. DAPI-stained cells were spotted onto a glass microscope slide and viewed under 100× oil immersion on a Nikon Eclipse-50 microscope. Images of at least 200 cells from each strain were captured using the same exposure settings with QCapture Pro software. This process was independently repeated three times for each strain. The percentages of cells containing mtDNA were determined, with a cell containing any extranuclear DAPI staining scored as containing mtDNA.

TEM

The TEM protocol was compiled using suggestions from Wright (2000). The *pcp1* strains were grown in 15 mL -His

2% raffinose media at 30°C overnight with shaking to reach an OD_{600} between 0.5 and 1. The cells were pelleted at 1,500*g* for 10 min at 18°C and the cell pellet resuspended in 15 mL YP 2% raffinose and returned to 30°C with continuous shaking for 1 h. Each culture was fixed with the addition of an equal volume of 4% gluteraldehyde in 2× piperazine-N,N′-bis(2-ethanesulfonic acid) (PIPES) buffer (0.2 M PIPES pH 6.8, 0.2 M sorbitol, 2 mM $MgCl_2$, 2 mM $CaCl_2$) for 5 min at room temperature followed by 2% gluteraldehyde in 1× PIPES buffer overnight at 4°C. Fixed cells were incubated in 2% potassium permanganate, washed with water, and dehydrated with a series of graded ethanol washes (35% ethanol, 50% ethanol, and 70% ethanol). The cells were incubated en bloc in 1% uranyl acetate in 70% ethanol overnight. Next day, the cells were twice washed for 15 min with 95% ethanol followed by four 15 min washes in 100% ethanol.

The cells were gradually infiltrated with resin replacing ethanol with acetone using 25% Spurr's Resin in 75% acetone, 50% Spurr's Resin in 50% acetone, and 75% Spurr's in 25% acetone overnight. Infiltration was completed in 100% resin for 24 h. The following day, cells were embedded in fresh Spurr's Resin in a 68–70°C oven overnight. The blocks were trimmed, sectioned, and placed onto copper mesh grids for staining in 2% alcoholic uranyl acetate followed by lead citrate. TEM was performed on a JEOL JEM-1230 electron microscope at 80 kV, 60 μA, 140–180pA/cm^2 using spot size three at a magnification of ×6,000–8,000 to image whole cells and ×12,000 to visualize individual mitochondria. Approximately 30 cells were photographed for each of the *pcp1* mutants.

Mitochondria isolation

The cells (2 L) were grown overnight in the appropriate selective media containing 2% raffinose at 30°C with continuous shaking. Mitochondria were isolated following published procedures as described (Murakami et al., 1988). The final mitochondrial pellet was resuspended in 1× buffer A (20 mM 4-(2-hydroxyethyl)-1-piperazineethanesulfonic acid [HEPES] pH 7.5, 0.6 M sorbitol, 10 U/mL trasylol, 1 mM p-aminobenzamidine, 0.1% bovine serum albumin, 1 mM phenylmethanesulfonylfluoride) and the mitochondrial protein content determined spectrophotometrically. Isolated mitochondria were diluted with an equal volume of 1× buffer A containing 20% dimethyl sulfoxide, aliquoted in 1–2 mg volumes, and stored at −80°C.

Sodium dodecyl sulfate PAGE (SDS-PAGE)

Isolated mitochondria were washed with 20 mM HEPES pH 7.4, 0.6 M sorbitol buffer and centrifuged at 20,400*g* for 2 min at 4°C. The mitochondrial pellets were resuspended in 20 mM HEPES pH 7.4, 0.6 M sorbitol buffer to achieve a concentration of 10 mg/mL. One hundred micrograms was added to 1× SDS loading buffer (300 mM Tris base, 4% SDS, 17% glycerol, 0.007% bromophenol blue, 90 mM dithiothreitol), sonicated, and heated at 55°C for 5 min. Proteins were separated by electrophoresis through a 12% or 15% discontinuous SDS polyacrylamide gel.

BN-PAGE

The following BN-PAGE protocol was modified based on various sources (Schägger and von Jagow, 1991; Schägger et al., 1994; Dekker et al., 1996; Wagner et al., 2010). One microgram of isolated mitochondria from selected strains were washed with 1 mL 20 mM HEPES pH 7.4, 0.6 M sorbitol buffer and centrifuged at 20,400*g* for 2 min at 4°C. Mitochondrial pellets were lysed in a 0.5% digitonin buffer (0.5% digitonin, 20 mM Tris-HCl pH 7.5, 1 mM EDTA, 50 mM NaCl, 10% glycerol, 1 mM phenylmethylsulfonyl fluoride) to obtain a protein concentration of 4 mg/mL at a detergent to protein ratio of 1.4:1 (g/g). Different detergent to protein ratios were obtained by varying the percent weight by volume of digitonin used in the lysis buffer (0.5% digitonin = 1.4:1 g, 0.25% digitonin = 0.7:1 g). A soluble protein fraction was then isolated by centrifugation at 100,000*g* for 30 min at 4°C. 5.5 μL of 10× loading buffer (5% Coomassie Blue G, 500 mM 6-aminocaporic acid, 100 mM Bis-Tris pH 7.0) was added to 200 μg of protein. After an additional spin at 20,400*g* for 2 min at 4°C, samples were either frozen at −20°C or immediately used. Samples were loaded onto a 3–13% blue native polyacrylamide gel and run at 4°C in 0.02% Coomassie Blue G-250, 50 mM tricine, 15 mM Bis-Tris pH 7.0 cathode buffer at 100 V for ~30 min, 160 V for about 3 h, and then 160 V in cathode buffer without Coomassie Blue G-250 for an additional 5 h. The resulting BN-PAGE was either used directly for determining ATP synthase activity using an in-gel activity assay or transferred to polyvinylidene fluoride (PVDF) membrane for immunoblotting.

Immunoblotting

The immunoblot analysis was carried out following established procedures (Harlow and Lane, 1988). BN gels were transferred to PVDF membrane, while SDS gels were transferred to nitrocellulose. Primary antibodies were used at the following dilutions: ATP-V α subunit at 1:5,000 (SDS) or 1:10,000 (BN-PAGE) (Cat# 459240, RRID: AB_2532234; Thermo Fisher Scientific); Hemagglutinin at 1:5,000 (Cat# MMS-101R, Antibody Registry: AB_291263; Covance); Ccp1p, Tom40p, and Tim11p at 1:8,000 (gift from Debkumar Pain, Rutgers University, NJ). Membranes were developed using horseradish peroxidase-conjugated secondary antibodies (Cat# NA9310 and NA934, Antibody Registry: AB_772193 and AB_772206; GE Healthcare) and

SuperSignal West Femto Chemiluminescence reagents (Thermo Fisher Scientific).

In-gel ATP synthase activity assay

Freshly processed mitochondrial proteins were separated by electrophoresis through a BN-PAGE, and the resulting gel was incubated with 20 mL ATP buffer (50 mM glycine-NaOH pH 8.4, 5 mM $MgCl_2$, 20 mM ATP) for 20 min at room temperature without shaking followed by 20 mL 10% $CaCl_2$ as described (Bornhövd et al., 2006). The positions of calcium phosphate precipitates were marked, a photo taken, and the gel incubated in destain solution (64% methanol, 3.1 M glacial acetic acid) overnight to visualize the protein standards.

Data analysis

The relative differences in protein levels were determined using ImageJ software with s-Mgm1p compared with Pgk1p and the ATP synthase α subunit and Tim11p levels compared to Tom40p. The resulting ratios were then normalized to that obtained for *PCP1*. Mitochondria cristae was quantified based on the ultrastructure present in TEM images. Area measurements for each mitochondrion were acquired using ImageJ software. The subsequent areas where binned into 20 nm^2 groupings for analysis. Statistical significance was calculated from measurements using a two-tailed *T* test assuming equal variances. The null hypothesis assumed the means from each *pcp1* strain was equal to the wild-type (*PCP1*) mean with a 95% confidence level ($\alpha = 0.05$).

Data obtained for mtDNA staining and Mgm1p processing was analyzed using a one-way analysis of variance with a post hoc Tukey's HSD test with statistical differences having a $P < 0.01$.

Results

pcp1 mutants exhibit a range of growth defects

We took advantage of the finding that yeast cells deleted for *PCP1* are unable to use nonfermentable carbon to sustain growth to identify alleles of *PCP1* that resulted in reduced function (Sesaki et al., 2003a). To this end, a haploid *pcp1* deletion strain transformed with a library of hydroxylamine mutagenized *PCP1* plasmid was screened for colonies that exhibited poor growth on ethanol/glycerol containing selective plates. After multiple rounds of screening, plasmid isolation, and retesting, five mutants were selected for further analysis (Figure SA1A). These mutants displayed a varying degree of growth defects and were found to contain nucleotide mutations that altered 1–2 amino acids in the *PCP1* open-reading frame. All mutants are referred to by single-letter code along with their numeric amino acid position and include: Pcp1p (G120D), Pcp1p (G233D), Pcp1p (S252N), Pcp1p (G315D), and Pcp1p (G233S V321A). These mutations are found in highly conserved regions of the protein (Figure SA1C) and are predicted to map to transmembrane helices (TMH) 1, 4, and 6, as well as a loop domain between helices 3 and 4 in the mature Pcp1 protein (Figure SA1B).

As an initial approach to compare the impact each *pcp1* mutation had on overall growth, a spotting assay was carried out. Variable growth defects were identified for the mutants under nonselective (glucose) and selective (ethanol-glycerol) testing conditions (Figure 1A). Least impaired was the Pcp1p (G233S V321A) mutant, followed by Pcp1p (G120R) and Pcp1p (S252N). The Pcp1p (G233D) mutant was found to have poor growth on ethanol-glycerol. The G315D mutant exhibited a growth pattern most similar to that of the Δ*pcp1* mutant, with reduced growth on glucose and no growth on ethanol-glycerol-containing plates suggesting that the mutant is likely a null allele. However, immunoblot analysis confirmed that Pcp1 protein was present in the G315D mutant, although at a reduced level compared with other mutants (Figure SA2).

Yeast having lost the ability to utilize nonfermentable carbon for growth are referred to as petites (Day, 2013). To quantify the differences in growth defects seen for *pcp1* mutants on ethanol-glycerol, the percentage of petites in an exponentially growing culture was determined using a replica printing approach. Similar to that seen by spotting, cultures of Δ*pcp1* and Pcp1p (G315D) were found to be 100% petite, while cultures of Pcp1p (G233S V321A) had a petite frequency similar to wild-type at ~2–3% (Figure 1B). The three remaining mutants, Pcp1p (S252N), Pcp1p (G120R), and Pcp1p (G233D), had calculated average petite frequencies of 14%, 59%, and 70%, respectively. Overall, the calculated petite frequencies matched the increased deficiencies seen for growth on ethanol-glycerol by spotting.

The absence of growth on nonfermentable carbon is often due to the acquisition of deletions in, or complete loss of, the mitochondrial genome (Contamine and Picard, 2000). To determine whether the petite phenotype seen for each mutant was due to the complete loss of the mitochondrial genome, the presence of mtDNA was scored by DAPI staining. The cells in wild type and Pcp1p (G233S V321A) mutant cultures had extranuclear staining in over 93% of the cells, consistent with the majority of the culture retaining respiratory competence (Figure 1C). However, ~75% of the cells expressing Pcp1p (G120R) or Pcp1p (G233D) had staining consistent with mtDNA, suggesting that the petite phenotype in these strains was primarily due to the accumulation of mutations or deletions in the mitochondrial genome. Even cultures of the nonfunctional *pcp1* mutants (Δ*pcp1* and G315D) had some cells that retained mtDNA staining despite all scoring phenotypically

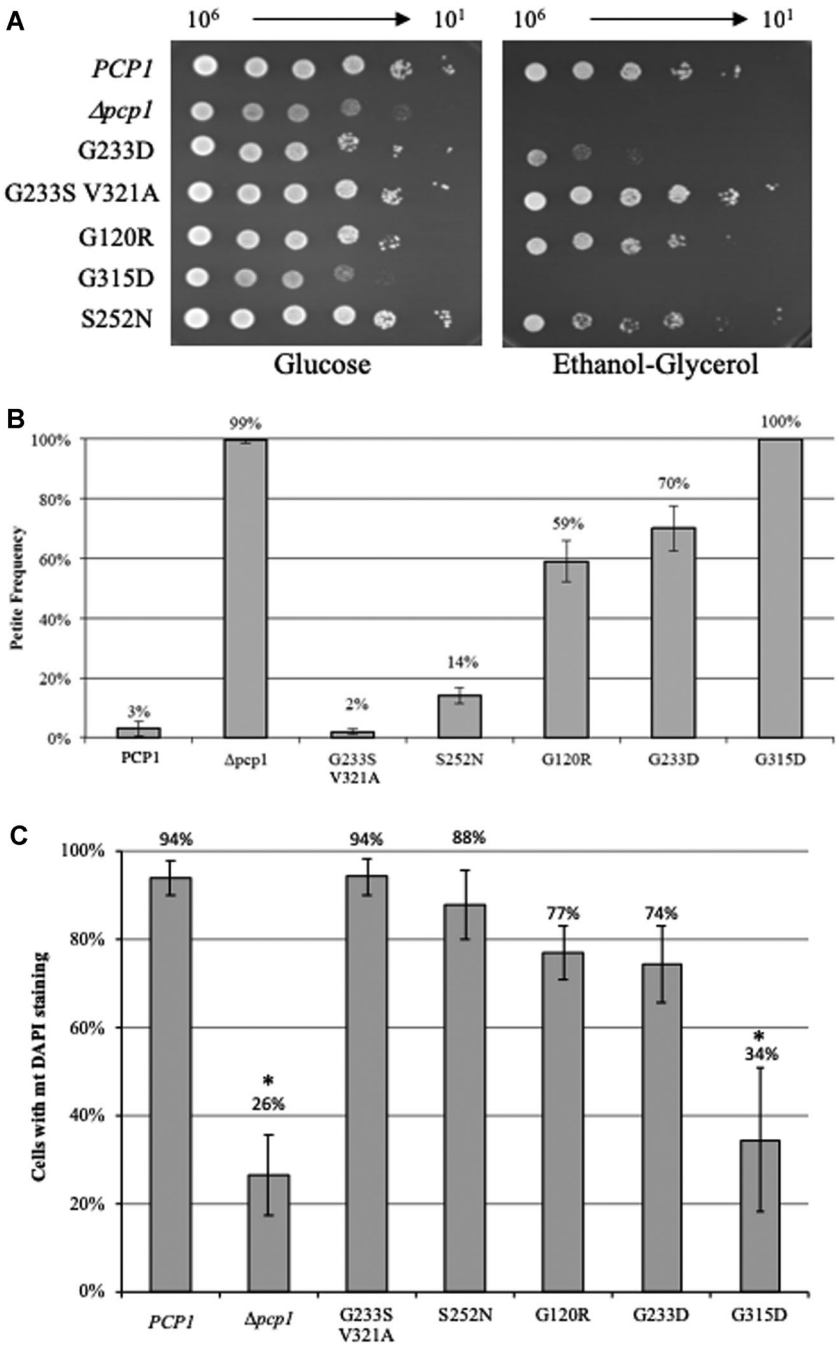

Figure 1 Reduced growth and loss of respiratory competence found for strains expressing mutant versions of *PCP1*. (A) Analysis of growth characteristics of haploid *pcp1* mutants under nonselective (glucose) and selective (ethanol-glycerol) conditions. A six-point 10-fold serial dilution spotting assay identifies *pcp1* mutants that are unable to support growth (Δ*pcp1* and G315D) or show reduced growth (G233D, S252N, and G120R) under selective conditions compared with *PCP1*. (B) Quantification of petite frequency reveals a range in respiratory competence. The difference in the number of cells in each culture that were able to grow on nonselective versus selective plates were determined for each strain with the average ± standard deviation reported for three independent experiments. (C) Quantification of 4′,6-diamidino-2-pheynlindole (DAPI) staining reveals a varying degree of extranuclear DNA staining for all *pcp1* mutants. Cells viewed by fluorescence microscopy identified mitochondrial DNA staining that correlated with petite frequency findings. Over 200 cells were counted for each strain with data presented as the average ± standard deviation for three independent experiments. Statistical significance was determined using a one-way analysis of variance (ANOVA) with a post hoc Tukey's HSD test, $*P < 0.01$.

as petites, data consistent with prior observations for *pcp1* deletion mutants (Herlan et al., 2003). The presence of mitochondrial DNA in these mutants were also supported by mitochondria-to-nuclear genome ratio data obtained by quantitative PCR (qPCR) analysis (Table SA1).

pcp1 mutants are defective in substrate processing

To identify the impact that each mutation had on Pcp1p activity, the processing of two Pcp1p substrates, Ccp1p and Mgm1p, was determined. In wild-type cells, Ccp1p is processed in two steps with Pcp1p activity catalyzing the final cleavage step to generate the mature form of the enzyme (Esser et al., 2002; Figure 2A, lane 1). In Δ*pcp1*, the second cleavage step does not take place, resulting in the accumulation of an intermediate form of Ccp1p (iCcp1p), and in our hands, a faster migrating form that is likely a degradation product. Of the 5 *pcp1* mutants, all retained some level of peptidase activity except for the Pcp1p (G315D) mutant, which primarily accumulated the intermediate form of Ccp1p. In wild-type cells, Mgm1p accumulates as both a long- and short-form (Figure 2B, lane 1) while only the long-form is found in Δ*pcp1* mutants (Herlan et al., 2003; Figure 2B, lane 2). Similar to that seen for Ccp1p processing, the Pcp1p (G315D) mutant appeared to essentially lack peptidase activity. While Mgm1p processing for the Pcp1p (G233S V321A) mutant was most similar to that of wild type, a significant reduction in the conversion of the long-to-short isoform of Mgm1p was identified for the three remaining mutants including Pcp1p (S252N), Pcp1p (G233D), and Pcp1p (G120R) (Figure 2C). Despite these differences in Mgm1p processing, no statistically significant differences in the total amount of Mgm1p protein was found. Altogether, the *pcp1* mutants exhibited defects in peptidase activity that correlated in severity with their growth patterns on ethanol-glycerol.

pcp1 mutants have a variable impact on mitochondrial morphology

A balance between the long and short isoforms of Mgm1p has been implicated in influencing mitochondrial fusion events in yeast (Herlan et al., 2003; Ishihara et al., 2006). Given the defects in Mgm1p processing detected for the *pcp1p* mutants, they are expected to impact mitochondrial morphology. The cursory analysis with fluorescence microscopy using mitochondrially targeted GFP or MitoTracker Orange CMTMRos found an increase in fragmented mitochondria for all of the Pcp1p mutants (data not shown; Xiao, 2013; Both and Gordon, 2015). To better define defects in mitochondrial architecture, TEM

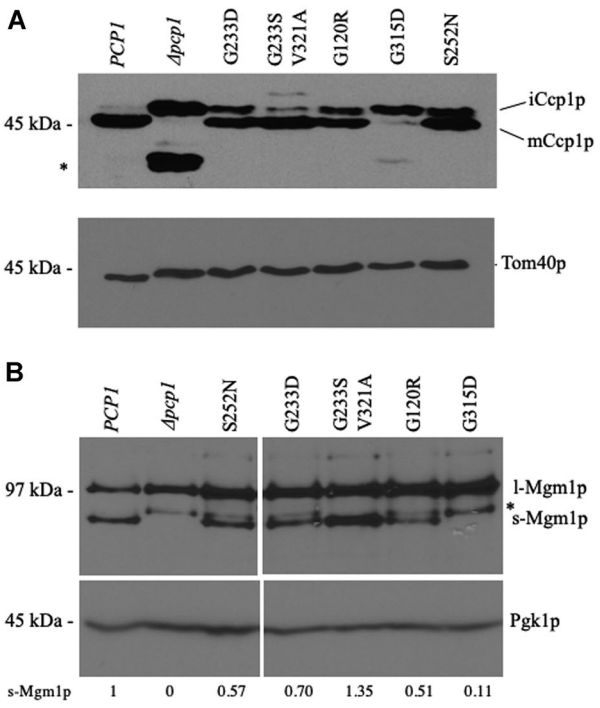

C

	s-Mgm1p	l-Mgm1p	* Mgm1p
PCP1	45 ± 2%	55 ± 3%	Not detected
Δ*pcp1*	Not detected	90 ± 6%**	10 ± 6%
S252N	26 ± 7%**	65 ± 1%	9 ± 6%
G233D	25 ± 10%**	64 ± 2%	11 ± 11%
G233S V321A	45 ± 4%	55 ± 4%	Not detected
G120R	23 ± 4%**	66 ± 2%*	11 ± 2%
G315D	5 ± 9%**	71 ± 6%**	24% ±7%

Figure 2 Pcp1p mutants exhibit reduced peptidase activity. (A) Differences in Pcp1p-mediated processing of Ccp1p were determined by immunoblot analysis of protein obtained from mitochondria isolated from the indicated strains. Complete processing of Ccp1p generates a mature form of the protein (mCcp1p) while defects in Pcp1p-mediated cleavage of Ccp1p results in the accumulation of a slower migrating intermediate form (iCcp1p). *Improperly processed form of Ccp1p. Tom40p was used to confirm equal lane loading (bottom panel). (B) Differences in Pcp1p-mediated processing of Mgm1p were determined by immunoblot analysis of total protein extracts isolated from the indicated strains. Mgm1p is present as a long- and short-form (l-Mgm1p and s-Mgm1p, respectively) with the conversion of the long- to short-form mediated by Pcp1p activity. Defects in Pcp1p peptidase activity result in reduced levels of s-Mgm1p and the accumulation of an improperly processed form of the protein (indicated with an asterisk; Schäfer et al., 2010). Pgk1p was used to confirm equal lane loading (bottom panel). The normalized amount of s-Mgm1p present in each mutant relative to Pgk1p is shown ($n = 3$). (C) The percent each form is of the total Mgm1p detected in each strain was determined following densitometric analysis. Data presented as the average ± standard deviation from three experiments. Values significantly different from *PCP1* are indicated. $*P < 0.05$, $**P < 0.01$.

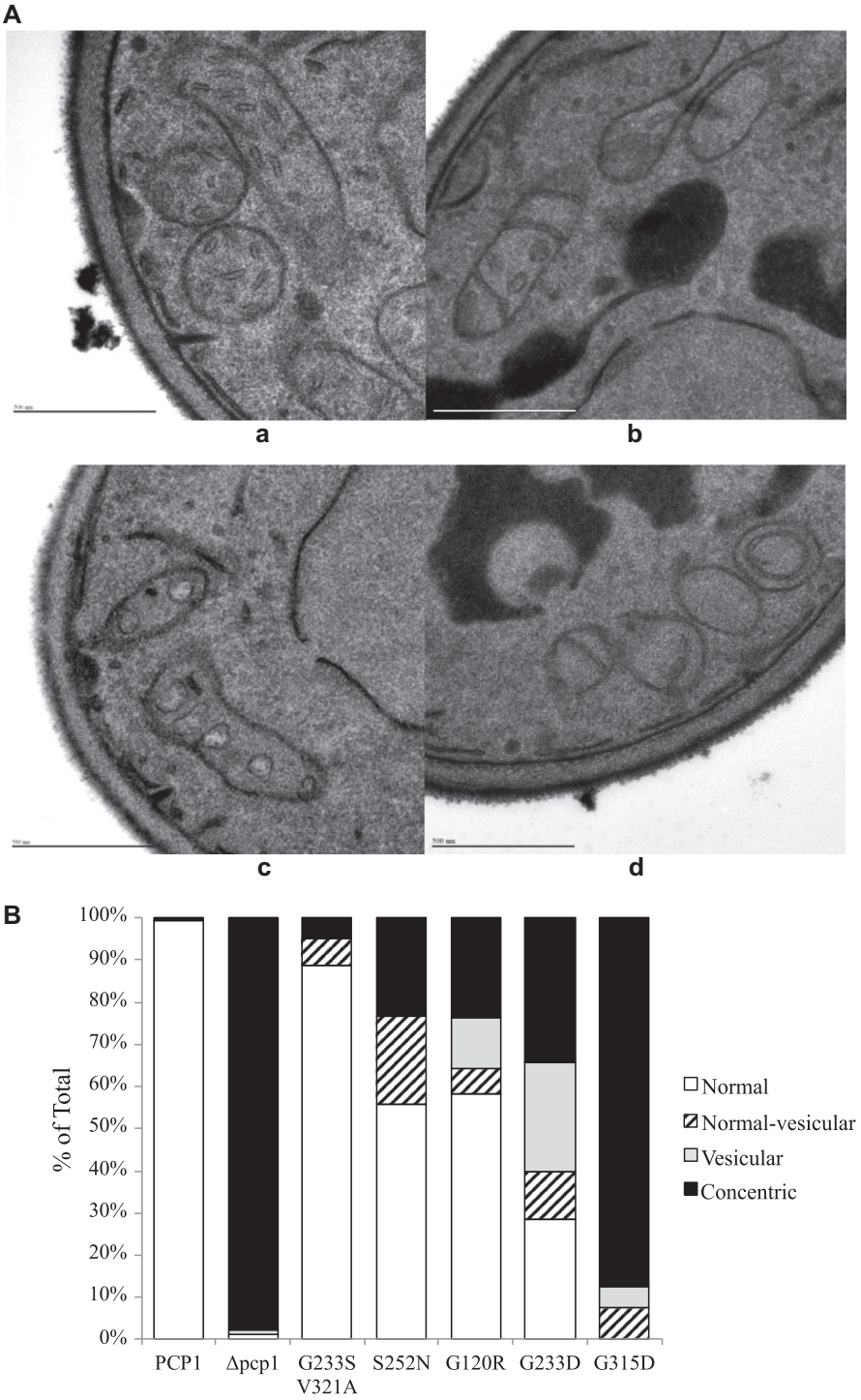

Figure 3 Mitochondrial cristae structure is disrupted in *pcp1* mutants as determined by transmission electron microscopy (TEM). A. Representative TEM images of cristae structures found include: (a) normal, (b) normal-vesicular, (c) vesicular, and (d) concentric. Images were taken at ×12,000 magnification; scale bars = 500 nm. (B) Distribution of mitochondrial cristae organization identified by TEM analysis for each strain. Graphical representation of cristae morphology found in wild-type (PCP1), the deletion mutant (Δpcp1), and each of the five *pcp1* mutant strains. Normal; white box, normal-vesicular; hatched box, vesicular; gray box, concentric; black box.

was used. The ultrastructure for all strains were analyzed and four different cristae categories were identified: normal, normal-vesicular, vesicular, and concentric (Sun et al., 2007) (Figure 3). Normal cristae are defined as those that had little intra-cristae space visible and often appeared to be protruding from the outer membrane as close proximity of the outer and inner membrane make it difficult to distinguish between the two (Figure 3a). Normal cristae were also fairly numerous and appeared to be the textbook example of wild-type mitochondrial morphology. The vesicular category was used to describe mitochondria, in which the mitochondrial inner membrane formed vesicle-like structures that did not appear to be attached to the outer membrane (Rabl et al., 2009) (Figure 3b). The mitochondria described as having normal-vesicular morphology had cristae with long inner membrane sheets that appeared to divide the mitochondria into sections that contained inner membrane vesicles (Figure 3c). The mitochondrial cristae morphology described as concentric contained mitochondria that contained no visible cristae or cristae that appeared "onion-like" as described in the literature (Paumard et al., 2002) (Figure 3d). Concentric cristae also contained almost no cristae junctions. All of the *pcp1* mutant strains contained multiple cristae types and many of the strains often contained a single cell with mitochondria having more than one cristae type.

The number of mitochondria in each cristae category was determined for each *pcp1* strain (Figure 3B). For the wild-type strain, the majority of the mitochondria were found to be normal (99.2%). Pcp1p (G233S V321A) also had the majority of its mitochondria in the normal category (88.7%). Pcp1p (S252N) and Pcp1p (G120R) both had a little over 50% normal mitochondria, while only 28.5% of the mitochondria in Pcp1p (G233D) were scored as normal. Cells deleted for *pcp1* or containing the Pcp1p (G315D) mutation had no mitochondria with normal ultrastructure. However, Pcp1p (G315D) may exhibit some peptidase activity as a few of the mitochondria were found to have retained some cristae ultrastructure (7.6% normal-vesicular and 4.8% vesicular), a conclusion that is supported by data presented in Figure 2. Pcp1p (G233S V321A) and Pcp1p (S252N) both contained levels of concentric and normal-vesicular mitochondria, although these occurred in greater numbers in Pcp1p (S252N). Both Pcp1p (G120R) and Pcp1p (G233D) contained all four mitochondrial cristae morphologies with Pcp1p (G233D) appearing to have a more severe impact on cristae organization as 71.5% of the mitochondria lacked normal cristae compared to 41.8% in Pcp1p (G120R).

To determine whether there were differences in mitochondrial size between *pcp1* mutants the area of each mitochondrion was measured. Only mitochondria believed to be in cross-section were analyzed for this purpose. The cross-sectional areas were measured for each strain and the data presented in Figures 4 and SA3. The majority of the mitochondria in Pcp1p (G233D), Pcp1p (S252N), and Pcp1p (G120R) were found within the 41–60 nm^2 range, consistent with the mitochondria found in the *PCP1* strain. Mitochondria in Pcp1p (G315D) ($P = 2.16 \times 10^{-18}$) and Δ*pcp1* ($P = 6.34 \times 10^{-21}$) had a significantly smaller cross-sectional

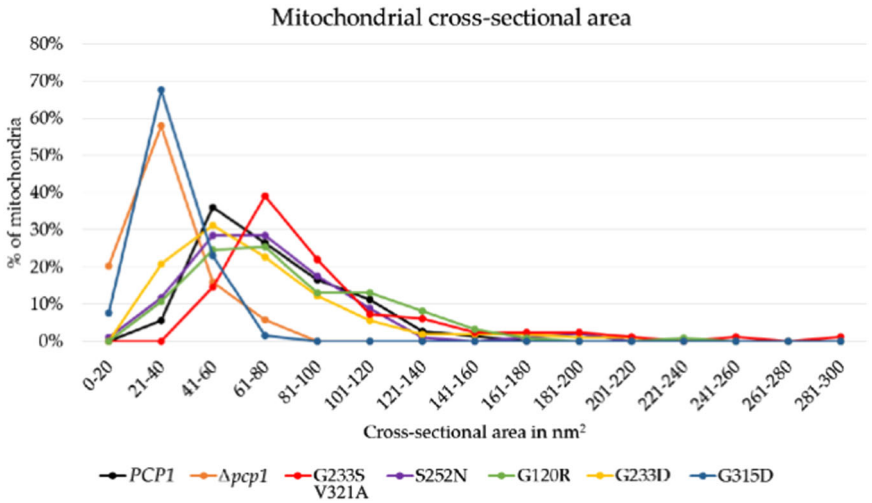

Figure 4 The analysis of mitochondrial cross-sectional area identifies differences in mitochondria size. Transmission electron microscopy (TEM) images were analyzed for mitochondria presented in cross-section and their area measured. Data were grouped into 20 nm^2 increments and the percentage of mitochondria in each group presented graphically. The number of mitochondria measured for each strain were as follows: *PCP1*; $n = 72$, Pcp1p (S252N); $n = 102$, Pcp1p (G233D); $n = 106$, Pcp1p (G120R); $n = 122$, Δ*pcp1*; $n = 69$, Pcp1p (G315D); $n = 65$, and Pcp1p (G233S V321A); $n = 82$.

Cell Biol Int **44** (2020) 200–215 © 2019 The Authors. *Cell Biology International* published by John Wiley & Sons Ltd on behalf of International Federation of Cell Biology

area falling within 21–40nm^2. This is consistent with Amutha et al. (2004) who described *Δmgm1* mitochondria as small, round, and lacking cristae folds. Surprisingly, the Pcp1p (G233S V321A) mutant was found to have a significantly larger mitochondria cross-sectional area, with the majority falling in the range of 61–80nm^2 ($P = 0.0002$).

ATP synthase and Tim11p steady-state levels are altered in pcp1 mutants

To understand how each of the Pcp1p mutants resulted in the accumulation of differently structured mitochondria, we focused on characterizing the oligomerization status of the ATP synthase complex in each mutant as it has been linked to cristae architecture (Paumard et al., 2002; Strauss et al., 2008; Davies et al., 2012). First, we measured the steady-state levels of the F_1 complex component, ATP synthase α, and a protein associated with the F_0 region of the ATP synthase complex, Tim11p (subunit *e*). Immunoblot analysis on isolated mitochondria found no significant differences in the levels of ATP synthase α subunit for Pcp1p (S252N), Pcp1p (G233D), Pcp1p (G233S V321A), and Pcp1p (G120R) when compared with a wild-type *PCP1* strain. However, *Δpcp1* ($P = 0.03$) and Pcp1p (G315D) ($P = 0.05$) had significantly lower levels of ATP synthase α subunit compared with wild type (Figures 5A and 5B). As previously reported, the *Δpcp1* mutant lacked detectable Tim11p (Amutha et al., 2004). The Pcp1p (G315D) also contained no detectable Tim11p, while Pcp1p (S252N), Pcp1p (G233D), and Pcp1p (G120R) had Tim11p levels not statistically different from wild type. Interestingly, the Pcp1p (G233S V321A) mutant was found to have higher Tim11p ($P = 0.008$) (Figures 5C and 5D).

pcp1 mutants decrease ATP synthase super-complex assembly and activity

Tim11p has been shown to be required for ATP synthase dimer formation and thus has a role in mitochondrial cristae formation (Arnold et al., 1997; Arselin et al., 2003; Amutha et al., 2004; Everard-Gigot et al., 2005; Bornhövd et al., 2006). To establish whether any of the Pcp1p mutations impacted the ability of ATP synthase to form dimers as well as higher-order complexes, mitochondrial lysates from each *pcp1* mutant was analyzed by BN-PAGE using conditions shown to separate ATP synthase into oligomers, dimers, and monomers (Paumard et al., 2002; Arselin et al., 2003; Bornhövd et al., 2006). To identify subtle differences in ATP synthase complex stability, we compared complexes formed using digitonin-to-protein ratios of 1.4:1 (g/g) and 0.7:1 (g/g) (Paumard et al., 2002). Pcp1p (G315D) was omitted from these experiments as no ATP synthase complexes were detected in this mutant (Figure SA4). Unlike Δ*pcp1*, each of the four *pcp1* mutants analyzed were found to have ATP synthase monomers as well as higher-order oligomeric complexes (Figure 6A). Consistent with the previous reports (Paumard et al., 2002), we found that a lower digitonin-to-protein ratio resulted in an increase in oligomeric forms when compared with the higher ratio with no significant differences in stability between the *pcp1* mutants.

To extend the immunoblot results, ATP synthase activity was determined using an in-gel activity assay (Figure 6C). Mitochondrial proteins were separated by BN-PAGE and ATP synthase activity determined through the formation of a P_i-calcium precipitate (Bornhövd et al., 2006). The migration position of the ATP synthase dimer was confirmed by its absence in the *Δtim11* strain (Arnold et al., 1998) while the relative sizes of the free F_1 and ATP synthase monomer were determined following destaining (Figure SA5) and were consistent with the literature (Arnold et al., 1998; Paumard et al., 2002). Surprisingly, the activity assay was found to be a more sensitive readout of ATP synthase complex assembly as in addition to identifying oligomeric, dimeric, and monomeric forms, free F_1 was also readily detected (Figure 6C). The *Δpcp1* and Pcp1p (G315D) mitochondria (Figure SA4B) were found to only contain free F_1 while all other *pcp1* mutants had ATP synthase activity associated with higher-order super-complexes. As expected, when comparing ATP synthase activity between the detergent ratios, an increase in oligomer activity was found using the lower digitonin-to-protein ratio (Figure 6C).

Discussion

A number of protein and protein complexes have been identified based on their role in organizing mitochondrial cristae. In budding yeast these include the inner membrane fusion protein Mgm1p, the F_1F_0 ATP synthase dimer, and the multi-subunit mitochondrial contact site and cristae organizing system (MICOS) complex (Strauss et al., 2008; Davies et al., 2012; Harner et al., 2016). In the case of Mgm1p, proteolytic processing of the polypeptide by the rhomboid peptidase, Pcp1p, has been shown to be critical for normal cristae formation (Herlan et al., 2003; Amutha et al., 2004). Targeted mutations that disrupt Pcp1p activity have been generated, primarily as an approach to confirm the catalytic site of the enzyme, focusing on the highly conserved serine and histidine residues at amino acid positions 256 and 313, respectively. Few mutations outside of these two regions have been analyzed (Esser et al., 2002; Sesaki et al., 2003a).

Using a random mutagenesis approach, coupled with a selection for reduced growth on a nonfermentable carbon source, we have identified additional amino acids within Pcp1p required for full peptidase activity. Two of these mutations mapped to an amino acid upstream and downstream to the catalytic dyad and included serine at

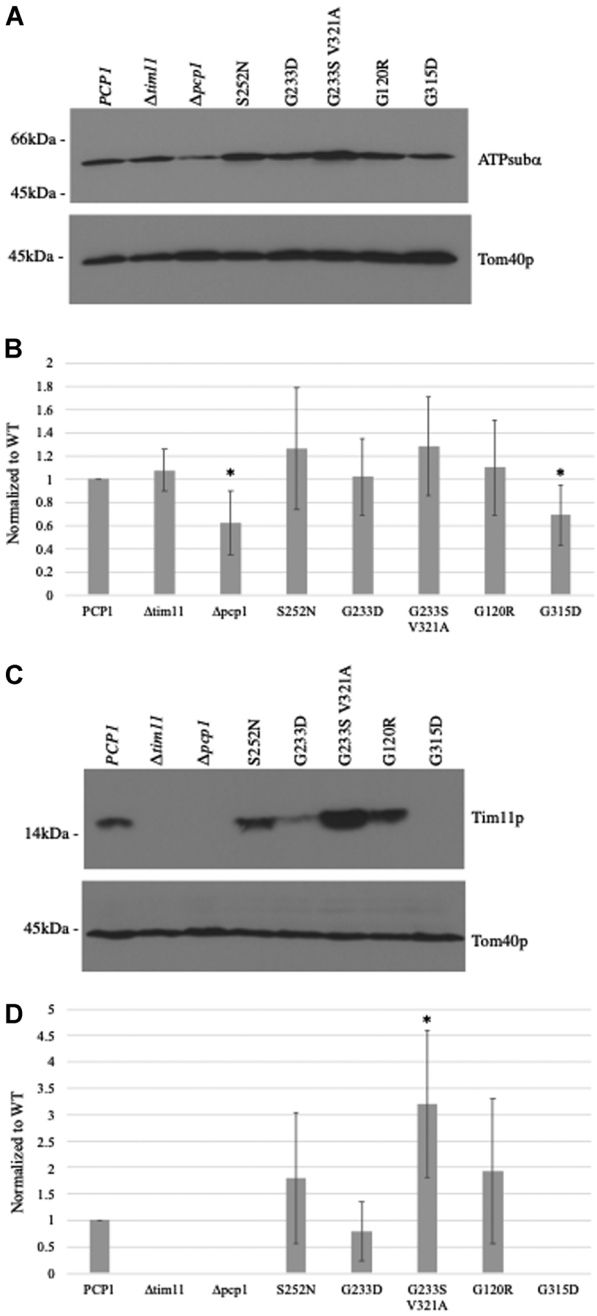

Figure 5 Pcp1p mutants have altered steady-state levels for select adenosine triphosphate (ATP) synthase subunits. (A) Nonfunctional *pcp1* alleles have reduced levels of ATP synthase α subunit. Proteins from isolated mitochondria were separated by sodium dodecyl sulfate polyacrylamide gel electrophoresis (SDS-PAGE) followed by immunoblot analysis using anti-ATPV α subunit and anti-Tom40 antibodies. Tom40p was used as a control to confirm equal loading of samples. (B) Densitometric analysis of the levels of ATP synthase α subunit relative to Tom40p and normalized to the *PCP1* wild-type control. Data presented as the average ± standard deviation from four experiments. $*P = 0.03$ for Δ*pcp1* and 0.05 for G315D). (C) Tim11p levels vary across the *pcp1* mutants. Proteins isolated as described above were analyzed by immunoblot for Tim11p and anti-Tom40 levels. (D) Densitometric analysis of the level of Tim11p relative to Tom40p and normalized to the *PCP1* wild-type strain. Data represent the average ± standard deviation from six experiments. $*P = 0.008$.

Cell Biol Int **44** (2020) 200–215 © 2019 The Authors. *Cell Biology International* published by John Wiley & Sons Ltd on behalf of International Federation of Cell Biology

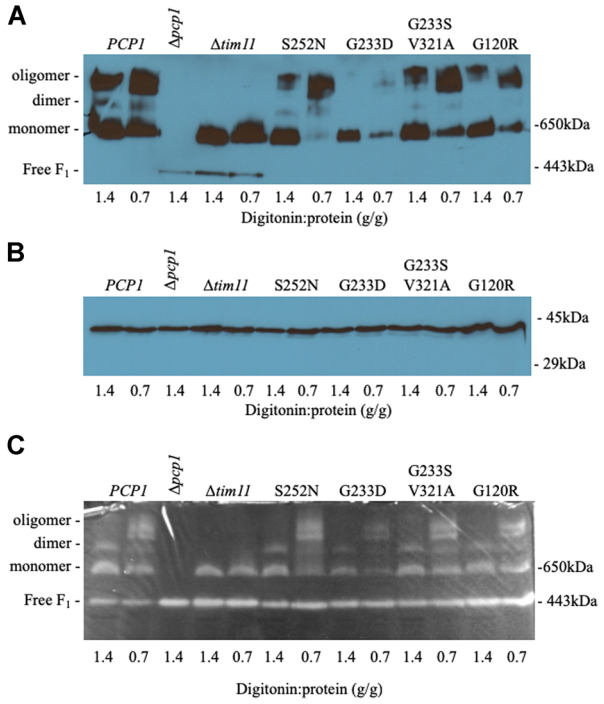

Figure 6 Nonfunctional *pcp1* alleles have reduced adenosine triphosphate (ATP) synthase super-complexes formed. ATP synthase complex oligomerization and ATPase activity were measured following blue native-polyacrylamide gel electrophoresis (PAGE). (A) Representative immunoblot showing ATP synthase oligomerization status using ATP synthase α subunit antibodies. Mitochondrial proteins from the strains indicated were solubilized in buffer at a digitonin to protein ratio of 1.4:1 (g/g) and 0.7:1 (g/g). (B) The corresponding sodium dodecyl sulfate PAGE (SDS-PAGE) of Tom40p levels by immunoblot analysis for samples presented in (A) confirm equal loading. (C) Representative in-gel ATP synthase activity for the same *pcp1* strains under the two solubilization conditions described above ($n = 3$).

position 252 and the glycine at position 315. Whereas the replacement of an isoleucine or an alanine for the serine had been reported previously to have no impact on Pcp1p function (Esser et al., 2002; Sesaki et al., 2003a), our data suggests that the introduction of an asparagine at position 252 interferes with the peptidase activity. Two additional amino acids important for Pcp1p activity that were identified in our screen included a glycine at positions 120 and 233. Interestingly, we isolated two different amino acid mutations at position 233 that varied in their severity with an aspartic acid less well tolerated than a serine. Sequence comparison of putative Pcp1p homologs from other fungi found glycine, alanine, or a serine at this position of the polypeptide (Figure SA1C), which may help explain the retention of functionality. However, given that this mutant also includes a second amino acid mutation at position 321, a valine to alanine, we cannot rule out the possibility that the effects that we have identified are due to the combined effect of these two alterations.

All of the *pcp1* mutants that we identified had reduced Pcp1p peptidase activity as measured by the altered ratio of short-to-long isoforms of Mgm1p (Figure 2). As shown previously, an imbalance in Mgm1p processing negatively impacts fusion of the mitochondrial inner membrane (Herlan et al., 2004). This is likely due to the different activities ascribed to each isoform with the long isoform responsible for tethering the fusion machinery to the inner membrane while the short isoform mediates the guanosine 5′-triphosphate (GTP)-dependent phospholipid rearrangement required for membrane bending and ultimately membrane fusion (Zick et al., 2009a; Rujiviphat et al., 2015). As expected, these *pcp1* mutants were found to vary in their accumulation of mitochondrial cristae structural defects with the severity in loss of cristae architecture correlating with the severity of Mgm1p processing deficiency. Given that the assembly of ATP synthase into dimers and higher-order oligomers has been shown to be important for the membrane curvature at the base of cristae (Paumard et al., 2002; Strauss et al., 2008; Davies et al., 2012), the assembly status of ATP synthase in the *pcp1* mutants was interrogated using BN-PAGE. Downstream analysis of oligomeric status by F_1 α-subunit western blot and ATPase activity assays were unable to identify ATP synthase complexes in the Pcp1p G315D mutant while a reduction in ATP synthase oligomers were found for the Pcp1p G233D mutant. These findings are consistent with the defects we identified in mitochondrial organization by electron microscopy. However, no substantial differences in ATP synthase assemblages were identified for the remaining *pcp1* mutants despite the accumulation of abnormal mitochondrial structures. Minor differences in the detection of ATP synthase complexes were noted when comparing immunoblot data with that of an ATPase activity assay. Generally, the F_1 α-subunit antibody was more sensitive at identifying ATP synthase oligomers at the higher digitonin: protein ratio compared to the ATPase assay, while the in-gel activity assay was more sensitive at detecting free F_1 subunits than by immunoblotting. These differences may be attributed to the variability of epitope accessibility to antibody recognition/binding under the native conditions used in BN-PAGE while for the ATPase activity assay the higher detergent levels may interfere with nucleotide binding or hydrolysis activities without disrupting the overall complex stability.

Despite identifying defects in mitochondrial organization for all of the *pcp1* mutants, even the most severe *pcp1* mutants (Δ*pcp1* and G315D) retained some level of detectable mitochondrial DNA suggesting that loss of cristae folds preceded the loss of the mitochondrial genome. These results are consistent with the findings of

Harner et al. (2016) using the *mgm1-5* temperature-sensitive mutant. Here, the authors found that only a short incubation at the nonpermissive temperature was required for loss of cristae morphology but the time period was likely too short as to have allowed for mtDNA loss. However, for each mutant a larger percentage of the cells were respiratory incompetent than would be predicted from the mitochondrial DNA staining data (Figures 1A and 1B) or qPCR analysis of genome ratios (Table S1), suggesting that defects in mitochondrial organization can give rise to nonfunctional mitochondrial genomes. This conclusion is confirmed by work from Osman et al. (2015) that found a yeast strain defective in mitochondrial fusion–fission activity accumulated deletions and rearrangements within the mitochondrial genome that resulted in loss of respiratory competence. The finding that ~25% of the cells expressing either the Pcp1p (G120R) or Pcp1p (G233D) mutation lacked detectable mtDNA by DAPI staining but had only a minor reduction in mitochondria:-nuclear genome ratios is also consistent with these cells acquiring mitochondrial genomic deletions. The absence of mtDNA by fluorescence microscopy may reflect a property of the mitochondrial nucleoids in these mutants, such as a structural alteration in mtDNA packaging that reduces DAPI binding, or simply an issue associated with resolving the cytoplasmic staining of mtDNA from that of the nucleus, a conclusion that would be supported by the observation that fusion deficient mitochondria are distributed throughout the cell rather than at the cell periphery (McQuibban et al., 2003).

In addition to having defects in cristae morphology, mitochondria in the Pcp1p (G315D) strain were found to have a smaller mitochondrial cross-sectional area than that of the wild-type strain. A similar decrease in mitochondrial size has been previously reported for *MGM1* mutants and for cells deleted for the outer membrane fusion protein *FZO1* (Hermann et al., 1998; Sesaki et al., 2003b; Amutha et al., 2004). A surprising result was finding a larger average mitochondrial cross-sectional area for the Pcp1 (G233S V321A) mutant compared with that of wild-type cells. This mutant also had elevated levels of the ATP synthase dimerization component, Tim11p without an appreciable difference in ATP synthase oligomerization. How could increased Tim11p levels impact mitochondrial architecture? Recent work has shown that Tim11p, as part of the ATP synthase dimer, physically associates with the MICOS component, Mic10 (Eydt et al., 2017; Rampelt et al., 2017). This interaction occurs outside of the cristae junction and involves a subpopulation of Mic10 that is not part of the larger MICOS complex.

In yeast, the MICOS complex is composed of six different protein components (Mic60, Mic19, Mic10, Mic26, Mic27, and Mic12) responsible for the formation and/or stabilization of cristae junctions (review; Quintana-Cabrera et al., 2018). MICOS functions as two sub-complexes. One sub-complex contains the core constituent, Mic60, a transmembrane protein shown to interact with proteins of the preprotein import and sorting pathways and therefore involved in the formation of outer and inner membrane contact sites (Harner et al., 2011; Hoppins et al., 2011; Zerbes et al., 2012). The second MICOS complex contains Mic10 whose membrane bending activity is responsible for cristae junction curvature (Barbot et al., 2015). Deletion of Mic60 or Mic10 results in the loss of cristae junctions and the formation of lamellar mitochondria structures (Bohnert et al., 2015; Eydt et al., 2017) and both are thought to influence F_1F_0-ATP synthase oligomerization (Rabl et al., 2009; Eydt et al., 2017; Rampelt et al., 2017). Therefore, it is tempting to speculate that the increased Tim11p in the Pcp1 (G233S V321A) mutant leads to an increase in Mic10 association with ATP synthase dimers, which, in turn, alters the balance for the roles of the MICOS complex and ATP synthase oligomers in cristae structure.

Changes in mitochondrial bioenergetics have been shown to influence Mgm1p processing providing a link between physiological parameters and mitochondrial structure (Herlan et al., 2004). The identification of Pcp1p mutants that vary in Mgm1p processing provide us with an additional tool to probe the link between these inner membrane complexes and cristae morphology.

Acknowledgments and funding

This work was supported by a grant from the National Institutes of Health (1R15GM085755-01A2) awarded to D.M.G. and by the Department of Biological Sciences startup funds. N.X. and M.E.H. were supported in part by a Department of Biological Sciences Teaching Assistantship. The authors thank Amanda Lawrence and the Institute for Imaging and Analytical Technologies at Mississippi State University for help with transmission electron microscopy and Dr. Debkumar Pain for the gift of Ccp1p and Tom40p antibodies.

Author contribution

D.M.G. conceived and designed the experiments; N.X., M.E.H., A.P.B., and D.M.G. performed the experiments; N.X., M.E.H., A.P.B., and D.M.G. analyzed the data; M.E.H. and D.M.G. wrote the paper; M.E.H., A.P.B, and D.M.G. edited the paper.

Conflict of interest

The authors declare no conflict of interest. The funding sponsors had no role in the design of the study; in the

collection, analyses, or interpretation of data; in the writing of the manuscript; and in the decision to publish the results.

ORCID

Donna M. Gordon http://orcid.org/0000-0003-3432-6685

References

Ackerman SH, Tzagoloff A (2005) Function, structure, and biogenesis of mitochondrial ATP synthase. Prog Nucleic Acid Res Mol Biol 80: 95–133, https://doi.org/10.1016/S0079-6603(05)80003-0

Amutha B, Gordon DM, Gu Y, Pain D (2004) A novel role of Mgm1p, a dynamin-related GTPase, in ATP synthase assembly and cristae formation/maintenance. Biochem J 381(1): 19–23, https://doi.org/10.1042/BJ20040566

Arnold I, Bauer MF, Brunner M, Neupert W, Stuart RA (1997) Yeast mitochondrial F1F0-ATPase: the novel subunit e is identical to Tim11. FEBS Lett 411(2–3): 195–200, https://doi.org/10.1016/s0014-5793(97)00691-1

Arnold I, Pfeiffer K, Neupert W, Stuart RA, Schagger H (1998) Yeast mitochondrial F1Fo-ATP synthase exists as a dimer: identification of three dimer-specific subunits. EMBO J 17(24): 7170–8, https://doi.org/10.1093/emboj/17.24.7170

Arselin G, Giraud M-F, Dautant A, Vaillier J, Brèthes D, Coulary-Salin B, Schaeffer J, Velours J (2003) The GxxxG motif of the transmembrane domain of subunit e is involved in the dimerization/oligomerization of the yeast ATP synthase complex in the mitochondrial membrane. Eur J Biochem 270(8): 1875–84, https://doi.org/10.1046/j.1432-1033.2003.03557.x

Barbot M, Jans Daniel C, Schulz C, Denkert N, Kroppen B, Hoppert M, Jakobs S, Meinecke M (2015) Mic10 oligomerizes to bend mitochondrial inner membranes at cristae junctions. Cell Metab 21(5): 756–63, https://doi.org/10.1016/j.cmet.2015.04.006

Bohnert M, Zerbes RM, Davies KM, Mühleip AW, Rampelt H, Horvath SE, Boenke T, Kram A, Perschil I, Veenhuis M, Kühlbrandt W, van der Klei IJ, Pfanner N, van der Laan M (2015) Central role of Mic10 in mitochondrial contact site and cristae organizing system. Cell Metab 21(5): 747–55, https://doi.org/10.1016/j.cmet.2015.04.007

Bornhövd C, Vogel F, Neupert W, Reichert AS (2006) Mitochondrial membrane potential is dependent on the oligomeric state of F1F0-ATP synthase supracomplexes. J Biol Chem 281(20): 13990–8.

Both P, Gordon DM (2015) The impact of Pcp1p mutations have on mitochondrial genome stability and morphology. J Miss Acad Sci 60: 23.

Chandel NS (2014) Mitochondria as signaling organelles. BMC Biol 12(1): 34, https://doi.org/10.1186/1741-7007-12-34

Cogliati S, Frezza C, Soriano Maria E, Varanita T, Quintana-Cabrera R, Corrado M, Cipolat S, Costa V, Casarin A, Gomes Ligia C, Perales-Clemente E, Salviati L, Fernandez-Silva P, Enriquez Jose A, Scorrano L (2013) Mitochondrial cristae shape determines respiratory chain supercomplexes assembly and respiratory efficiency. Cell 155(1): 160–71, https://doi.org/10.1016/j.cell.2013.08.032

Contamine V, Picard M (2000) Maintenance and integrity of the mitochondrial genome: a plethora of nuclear genes in the budding yeast. Microbiol Mol Biol Rev 64(2): 281–315.

Davies KM, Anselmi C, Wittig I, Faraldo-Gómez JD, Kühlbrandt W (2012) Structure of the yeast F1F0-ATP synthase dimer and its role in shaping the mitochondrial cristae. Proc Natl Acad Sci USA 109(34): 13602–7, https://doi.org/10.1073/pnas.1204593109

Day M (2013) Yeast petites and small colony variants: for everything there is a season. Adv Appl Microbiol 85: 1–41, https://doi.org/10.1016/B978-0-12-407672-3.00001-0

Dekker P, Müller H, Rassow J, Pfanner N (1996) Characterization of the preprotein translocase of the outer mitochondrial membrane by blue native electrophoresis. Biol Chem 377(7–8): 535–8.

Esser K, Tursun B, Ingenhoven M, Michaelis G, Pratje E (2002) A novel two-step mechanism for removal of a mitochondrial signal sequence involves the mAAA complex and the putative rhomboid protease Pcp1. J Mol Biol 323(5): 835–43, https://doi.org/10.1016/s0022-2836(02)01000-8

Everard-Gigot V, Dunn CD, Dolan BM, Brunner S, Jensen RE, Stuart RA (2005) Functional analysis of subunit e of the F1F0-ATP synthase of the yeast *Saccharomyces cerevisiae*: importance of the N-terminal membrane anchor region. Eukaryot Cell 4(2): 346–55, https://doi.org/10.1128/EC.4.2.346-355.2005

Eydt K, Davies KM, Behrendt C, Wittig I, Reichert AS (2017) Cristae architecture is determined by an interplay of the MICOS complex and the F1F0 ATP synthase via Mic27 and Mic10. Microb Cell 4(8): 259–72, https://doi.org/10.15698/mic2017.08.585

Giraud M-F, Paumard P, Soubannier V, Vaillier J, Arselin G, Salin B, Schaeffer J, Brèthes D, di Rago J-P, Velours J (2002) Is there a relationship between the supramolecular organization of the mitochondrial ATP synthase and the formation of cristae? Biochim Biophys Acta Bioenerg 1555(1): 174–80, https://doi.org/10.1016/S0005-2728(02)00274-8

Guan K, Farh L, Marshall TK, Deschenes RJ (1993) Normal mitochondrial structure and genome maintenance in yeast requires the dynamin-like product of the MGM1 gene. Curr Genet 24(1-2): 141–148.

Harlow E, Lane D (1988) Antibodies, a laboratory manual. Spring Harbor, NY: Cold Spring Harbor Laboratory Press.

Harner M, Körner C, Walther D, Mokranjac D, Kaesmacher J, Welsch U, Griffith J, Mann M, Reggiori F, Neupert W (2011) The mitochondrial contact site complex, a determinant of mitochondrial architecture. EMBO J 30(21): 4356–70.

Harner ME, Unger A-K, Geerts WJ, Mari M, Izawa T, Stenger M, Geimer S, Reggiori F, Westerman B, Neupert W (2016) An evidence based hypothesis on the existence of two pathways of mitochondrial crista formation. eLife 5: e18853, https://doi.org/10.7554/eLife.18853.001

Herlan M, Borhnhövd C, Hell K, Neupert W, Reichert AS (2004) Alternative topogenesis of Mgm1 and mitochondrial mor-

phology depend on ATP and a functional import motor. J Cell Biol 165(2): 167–73, https://doi.org/10.1083/jcb.200403022

Herlan M, Vogel F, Bornhovd C, Neupert W, Reichert AS (2003) Processing of Mgm1 by the rhomboid-type protease Pcp1 is required for maintenance of mitochondrial morphology and of mitochondrial DNA. J Biol Chem 278(30): 27781–8, https://doi.org/10.1074/jbc.M211311200

Hermann GJ, Thatcher JW, Mills JP, Hales KG, Fuller MT, Nunnari J, Shaw JM (1998) Mitochondrial fusion in yeast requires the transmembrane GTPase Fzo1p. J Cell Biol 143(2): 359–73.

Hoppins S, Collins SR, Cassidy-Stone A, Hummel E, DeVay RM, Lackner LL, Westermann B, Schuldiner M, Weissman JS, Nunnari J (2011) A mitochondrial-focused genetic interaction map reveals a scaffold-like complex required for inner membrane organization in mitochondria. J Cell Biol 195(2): 323–40, https://doi.org/10.1083/jcb.201107053

Ishihara N, Fujita Y, Oka T, Hihara K (2006) Regulation of mitochondrial morphology through proteolytic cleavage of OPA1. EMBO J 25(13): 2966–77, https://doi.org/10.1038/sj.emboj.7601184

Longtine MS, McKenzie A, III, Demarini DJ, Shah NG, Wach A, Brachat A, Philippsen P, Pringle JR (1998) Additional modules for versatile and economical PCR-based gene deletion and modification in *Saccharomyces cerevisiae*. Yeast 14(10): 953–61https://doi.org/.

Mannella CA, Pfeiffer DR, Bradshaw PC, Moraru II, Slepchenko B, Loew LM, Hsieh C, Buttle K, Marko M (2008) Topology of the mitochondrial inner membrane: dynamics and bioenergetic implications. IUBMB Life 52(3–5): 93–100, https://doi.org/10.1080/15216540152845885

McQuibban GA, Saurya S, Freeman M (2003) Mitochondrial membrane remodelling regulated by a conserved rhomboid protease. Nature 423(6939): 537–41, https://doi.org/10.1038/nature01633

Michaelis G, Esser K, Tursun B, Stohn JP, Hanson S, Pratje E (2005) Mitochondrial signal peptidases of yeast: the rhomboid peptidase Pcp1 and its substrate cytochrome c peroxidase. Gene 354: 58–63, https://doi.org/10.1016/j.gene.2005.04.020

Murakami H, Pain D, Blobel G (1988) The 70-kD heat shock-related protein is one of at least two distinct cytosolic factors stimulating protein import into mitochondria. J Cell Biol 107(6): 2051–7, https://doi.org/10.1083/jcb.107.6.2051

Nunnari J, Marshall WF, Straight A, Murray A, Sedat JW, Walter P (1997) Mitochondrial transmission during mating in *Saccharomyces cerevisiae* is determined by mitochondrial fusion and fission and the intramitochondrial segregation of mitochondrial DNA. Mol Biol Cell 8(7): 1233–42, https://doi.org/10.1091/mbc.8.7.1233

Osman C, Noriega TR, Okreglak V, Fung JC, Walter P (2015) Integrity of the yeast mitochondrial genome, but not its distribution and inheritance, relies on mitochondrial fission and fusion. Proc Natl Acad Sci USA 112(9): E947–56, https://doi.org/10.1073/pnas.1501737112

Paumard P, Vaillier J, Coulary B, Schaeffer J, Soubannier V, Mueller DM, Brèthes D, di Rago J-P, Velours J (2002) The ATP synthase is involved in generating mitochondrial cristae morphology. EMBO J 21(3): 221–30, https://doi.org/10.1093/emboj/21.3.221

Quintana-Cabrera R, Mehrotra A, Rigoni G, Soriano ME (2018) Who and how in the regulation of mitochondrial cristae shape and function. Biochem Biophys Res Commun 500(1): 94–101, https://doi.org/10.1016/j.bbrc.2017.04.088

Rabl R, Soubannier V, Scholz R, Vogel F, Mendl N, Vasiljev-Neumeyer A, Körner C, Jagasia R, Keil T, Baumeister W, Cyrklaff M, Neupert W, Reichert AS (2009) Formation of cristae and crista junctions in mitochondria depends on antagonism between Fcj1 and Su e/g. J Cell Biol 185(6): 1047–63, https://doi.org/10.1083/jcb.200811099

Rafelski SM, Viana MP, Zhang Y, Chan Y-HM, Thorn KS, Yam P, Fung JC, Li H, Costa LdF, Marshall WF (2012) Mitochondrial network size scaling in budding yeast. Science 338(6108): 822–4, https://doi.org/10.1126/science.1225720

Rampelt H, Bohnert M, Zerbes RM, Horvath SE, Warscheid B, Pfanner N, van der Laan M (2017) Mic10, a core subunit of the mitochondrial contact site and cristae organizing system, interacts with the dimeric F1F0-ATP synthase. J Mol Biol 429(8): 1162–70, https://doi.org/10.1016/j.jmb.2017.03.006

Rose MD, Fink GR (1987) KAR1, a gene required for function of both intranuclear and extranuclear microtubules in yeast. Cell 48(6): 1047–60, https://doi.org/10.1016/0092-8674(87)90712-4

Rothstein R (1991) Targeting, disruption, replacement, and allele rescue: integrative DNA transformation in yeast. Methods Enzymol 194: 281–301, https://doi.org/10.1016/0076-6879(91)94022-5

Rujiviphat J, Wong MK, Won A, Shih YL, Yip CM, McQuibban GA (2015) Mitochondrial genome maintenance 1 (Mgm1) protein alters membrane topology and promotes local membrane bending. J Mol Biol 427(16): 2599–609, https://doi.org/10.1016/j.jmb.2015.03.006

Schäfer A, Zick M, Kief J, Steger M, Heide H, Duvezin-Caubet S, Neupert W, Reichert AS (2010) Intramembrane proteolysis of Mgm1 by mitochondrial rhomboid protease is highly promiscuous regarding the sequence of the cleaved hydrophobic segment. J Mol Biol 401(2): 182–93, https://doi.org/10.1016/j.jmb.2010.06.014

Schägger H, Cramer WA, von Jagow G (1994) Analysis of molecular masses and oligomeric states of protein complexes by blue native electrophoresis and isolation of membrane protein complexes by two-dimensional native electrophoresis. Anal Biochem 217(2): 220–30, https://doi.org/10.1006/abio.1994.1112

Schägger H, von Jagow G (1991) Blue native electrophoresis for isolation of membrane protein complexes in enzymatically active form. Anal Biochem 199(2): 223–31, https://doi.org/10.1016/0003-2697(91)90094-A

Schiestl RH, Gietz RD (1989) High efficiency transformation of intact yeast cells using single stranded nucleic acids as carrier. Curr Genet 16(5–6): 339–46, https://doi.org/10.1007/BF00340712

Sesaki H, Jensen RE (1999) Division versus fusion: Dnm1p and Fzo1p antagonistically regulate mitochondrial shape. J Cell Biol 147(4): 699–706, https://doi.org/10.1083/jcb.147.4.699

Sesaki H, Southard S, Hobbs A, Jensen RE (2003a) Cells lacking Pcp1p/Ugo2p, a rhomboid-like protease required for Mgm1p processing, lose mtDNA and mitochondrial structure in a Dnm1p-dependent manner, but remain competent for mitochondrial fusion. Biochem Biophys Res Commun 308(2): 276–83, https://doi.org/10.1016/s0006-291x(03)01348-2

Sesaki H, Southard SM, Yaffe MP, Jensen RE (2003b) Mgm1p, a dynamin-related GTPase, is essential for fusion of the mitochondrial outer membrane. Mol Biol Cell 14(6): 2342–56, https://doi.org/10.1091/mbc.e02-12-0788

Sherman F (1991) Getting started with yeast. Methods Enzymol 194: 3–21, https://doi.org/10.1016/0076-6879(91)94004-v

Strauss M, Hofhaus G, Schröder RR, Kühlbrandt W (2008) Dimer ribbons of ATP synthase shape the inner mitochondrial membrane. EMBO J 27(7): 1154–60, https://doi.org/10.1038/emboj.2008.35

Sun MG, Williams J, Munoz-Pinedo C, Perkins GA, Brown JM, Ellisman MH, Green DR, Frey TG (2007) Correlated three-dimensional light and electron microscopy reveals transformation of mitochondria during apoptosis. Nat Cell Biol 9(9): 1057–65, https://doi.org/10.1038/ncb1630

Thomas D, Bron P, Weimann T, Dautant A, Giraud M-F, Paumard P, Salin B, Cavalier A, Velours J, Brèthes D (2008) Supramolecular organization of the yeast F1F0-ATP synthase. Biol Cell 100(10): 591–601, https://doi.org/10.1042/BC20080022

Wagner K, Perschil I, Fichter CD, van der Laan M (2010) Stepwise assembly of dimeric F1F0-ATP synthase in mitochondria involves the small F0-subunits k and i. Mol Biol Cell 21(9): 1494–504, https://doi.org/10.1091/mbc.E09-12-1023

Wong ED, Wagner JA, Gorsich SW, McCaffery JM, Shaw JM, Nunnari J (2000) The dynamin-related GTPase, Mgm1p, is an intermembrane space protein required for maintenance of fusion competent mitochondria. J Cell Biol 151(2): 341–52, https://doi.org/10.1083/jcb.151.2.341

Wong ED, Wagner JA, Scott SV, Okreglak V, Holewinske TJ, Cassidy-Stone A, Nunnari J (2003) The intramitochondrial dynamin-related GTPase, Mgm1p, is a component of a protein complex that mediates mitochondrial fusion. J Cell Biol 160(3): 303–11, https://doi.org/10.1083/jcb.200209015

Wright R (2000) Transmission electron microscopy of yeast. Microsc Res Tech 51(6): 496–510, https://doi.org/10.1002/1097-0029(20001215)51:6<496::AID-JEMT2>3.0.CO;2-9

Xiao N (2013) Genetic insights into the function of Pcp1p, a mitochondrial rhomboid protease. (Master of Science). Mississippi State University.

Yonetani T, Ohnishi T (1966) Cytochrome c peroxidase, a mitochondrial enzyme of yeast. J Biol Chem 241(12): 2983–4.

Zerbes RM, Bohnert M, Stroud DA, von der Malsburg K, Kram A, Oeljeklaus S, Warscheid B, Becker T, Wiedemann N, Veenhuis M, van der Klei IJ, Pfanner N, van der Laan M (2012) Role of MINOS in mitochondrial membrane architecture: cristae morphology and outer membrane interactions differentially depend on mitofilin domains. J Mol Biol 422(2): 183–91, https://doi.org/10.1016/j.jmb.2012.05.004

Zick M, Duvezin-Caubet S, Schäfer A, Vogel F, Neupert W, Reichert AS (2009a) Distinct roles of the two isoforms of the dynamin-like GTPase Mgm1 in mitochondrial fusion. FEBS Lett 583(13): 2237–43, https://doi.org/10.1016/j.febslet.2009.05.053

Zick M, Rabl R, Reichert AS (2009b) Cristae formation-linking ultrastructure and function of mitochondria. Biochim Biophys Acta 1793(1): 5–19, https://doi.org/10.1016/j.bbamcr.2008.06.013

SUPPORTING INFORMATION

Additional supporting information may be found online in the Supporting Information section at the end of the article.

Received 30 May 2019; accepted 18 August 2019.
Final version published online 3 September 2019.